

1 **MICROCLIMC: A MECHANISTIC MODEL OF ABOVE, BELOW AND WITHIN-CANOPY MICROCLIMATE**

2 **Ilya M. D. Maclean<sup>1,\*</sup> and David H. Klinges<sup>2,3</sup>**

3 <sup>1</sup>Environment and Sustainability Institute, University of Exeter Penryn Campus, Penryn, United  
4 Kingdom, TR13 9FG

5 <sup>2</sup>School of Natural Resources and Environment, University of Florida, Gainesville, FL, USA

6 <sup>3</sup>Smithsonian Environmental Research Center, Edgewater, MD, USA

7 \*Corresponding author: email: [i.m.d.maclean@exeter.ac.uk](mailto:i.m.d.maclean@exeter.ac.uk); Tel: +44(0)1326 255 968

8

9 **HIGHLIGHTS**

- 10
- 11 • Climate experienced by organisms differs from data used in most ecological studies, which  
12 typically use data derived from weather stations.
  - 13 • We present an ecologically-relevant model for predicting the climate experienced by  
14 organisms.
  - 15 • The model uses first-principles physics and can thus be applied in any terrestrial environment.
  - 16 • The model was verified and validated with data from four widely geographically distributed  
17 forest sites.
  - 18 • The model provides reasonably accurate estimates of microclimate.

18

19 **ABSTRACT**

20 Climate strongly influences ecological patterns and processes at scales ranging from local to global.  
21 Studies of ecological responses to climate usually rely on data derived from weather stations, where  
22 temperature and humidity may differ substantially from that in the microenvironments in which  
23 organisms reside. To help remedy this, we present a model that leverages first principles physics to  
24 predict microclimate above, within, and below the canopy in any terrestrial location on earth, made  
25 freely available as an R software package. The model can be run in one of two modes. In the first, heat  
26 and vapour exchange within and below canopy are modelled as transient processes, thus accounting for  
27 fine temporal-resolution changes. In the second, steady-state conditions are assumed, enabling  
28 conditions at hourly intervals or longer to be estimated with greater computational efficiency. We  
29 validated both modes of the model with empirical below-canopy thermal measurements from several  
30 locations globally, resulting in hourly predictions with mean absolute error of 2.77°C and 2.79°C for  
31 the transient and steady-state modes respectively. Alongside the microclimate model, several functions  
32 are provided to assist data assimilation, as well as different parameterizations to capture a variety of

33 habitats, allowing flexible application even when little is known about the study location. The model's  
34 modular design in a programming language familiar to ecological researchers provides easy access to  
35 the modelling of site-specific climate forcing, in an attempt to more closely unify the fields of  
36 micrometeorology and ecology.

37 **Key words:** temperature, climate, mechanistic model, biophysical ecology, evapotranspiration, R  
38 package.

39

## 40 1. INTRODUCTION

41 Temperature and water availability influence almost every ecological pattern and process, from the  
42 chemical reactions that control photosynthesis (Ingenhousz, 1779; Kumarathunge et al., 2019), to the  
43 global distribution of biomes (Gardner et al., 2020; Geiger, 1954; Köppen, 1884). Over the last two  
44 centuries thousands of ecological studies have investigated relationships between organisms and  
45 climate and one of the great challenges in modern ecology is to predict responses to climate change. A  
46 common feature of many of these studies is that the climate data used are derived or modelled from  
47 weather station data (Bramer et al., 2018; Potter et al., 2013). The microclimatic conditions experienced  
48 by organisms can differ vastly from the conditions ~1.5 m above the ground, measured inside a weather  
49 station screen (Maclean et al., 2019; Suggitt et al., 2011). Consequently, meteorological data will often  
50 incorrectly predict physical exposure to critical climate thresholds and the timing of climate-sensitive  
51 biological events (Baker, 1980; Perez and Feeley 2020). Microclimatic conditions in low-lying  
52 vegetation are also far more spatially and temporally variable than inside weather stations (Bennie et  
53 al., 2008; Lenoir et al., 2017), implying that the climatic niches of species, fundamental to predicting  
54 their distributions changes, cannot be accurately established by the methods normally used. Neglecting  
55 this variability, which can provide microrefugia or allow for thermoregulation, can also lead to  
56 overestimation of extinction rates (Suggitt et al., 2018). There is thus a clear need to develop methods  
57 that estimate microclimatic conditions of the environments in which organisms reside.

58

59 In fields outside ecology, the modelling of microclimates has a long history. Many of the methods used  
60 still owe their origins to the pioneering work by Richardson (1922), who demonstrated the basic laws  
61 of turbulent mixing in the surface layer of the atmosphere. In the 1950s, Monin & Obukhov (1954),  
62 extended this platform and, building on work by Prandtl (1925), provided a generalised, universal  
63 method for characterising wind speed and temperature profiles above the surface of a vegetation canopy  
64 under non-neutral conditions. The methods developed by these earlier pioneers in microclimatology  
65 still form the basis of most models that are in use today (see e.g. Ali et al., 2018; Bruse, 2014).  
66 Ecologists, however, have been surprisingly slow to adopt these more mechanistic approaches, and  
67 there is a still a tendency to derive microclimatic surfaces using statistical approaches (Fick and

68 Hijmans, 2017; Greiser et al., 2018; Meineri and Hylander, 2017). While potentially very good at  
69 capturing spatial variation in microclimate, the potential for models fitted using statistical inference to  
70 forecast novel conditions is somewhat questionable (Buckley et al., 2018; Evans, 2012; Nabi, 1985).

71

72 Nevertheless, the last few years have witnessed renewed ecological interest in microclimatology  
73 (Bramer et al., 2018; Lembrechts et al., 2019; Potter et al., 2013), in part driven by the availability of  
74 models written using programming languages with which ecologists are familiar (Lembrechts and  
75 Lenoir, 2019). One of the most widely used microclimate models in ecology, that of Porter *et al.* (1973),  
76 has been incorporated into the R package ‘NicheMapR’ (Kearney and Porter, 2017). Although flexible  
77 and widely tested, it requires pre-adjustment of input forcing to account for terrain and canopy shading  
78 effects as well as mesoclimatic processes such as elevation and cold air drainage. It is also designed to be  
79 run for single point locations. Building on the model of Bennie *et al.* (2008), Maclean *et al.* (2017)  
80 developed methods for modelling mesoclimatic effects, released as an R-package ‘microclima’, which  
81 is able to produce gridded estimates of microclimate (Maclean et al., 2019). Both models have  
82 subsequently been combined into a single framework (Kearney et al., 2020) and have also been  
83 developed for application in forecasting future climate (Maclean, 2020). Importantly, however, they  
84 were designed primarily for modelling above-canopy microclimate, and have principally been applied  
85 to determine microclimatic conditions over short vegetation. The environmental physics underpinning  
86 the models are associated with exchange above a vegetated surface and do not explicitly consider the  
87 microclimate within canopies. However, tropical forests alone host at least two-thirds of the worlds  
88 terrestrial biodiversity (Gardner et al., 2009), and with the exception of soil biota, the majority of  
89 remaining species spend at least some of their time among vegetated canopies (Lowman et al., 1996;  
90 Nakamura et al., 2017). In addition, thermal tolerances of plants are more sensitive to leaf temperatures  
91 than ambient air temperatures (Michaletz et al., 2016; Perez and Feeley 2020) and critical thermal  
92 thresholds can vary even within the canopy of a single tree (Curtis et al., 2019). Means of determining  
93 the microclimatic conditions across and below the canopy are therefore much needed.

94

95 In contrast to above the canopy, however, the physics of microclimate below-canopy is not fully  
96 resolved. Above-canopy, the transport of heat and vapour can accurately be described from estimates  
97 of atmospheric turbulence using *K*-theory (i.e. using a flux gradient approach). Emerging understanding  
98 (see e.g. Baneree *et al.*, 2017), suggests that *K*-theory often fails to describe turbulent transport in plant  
99 canopies. Many of its assumptions are violated because within-canopy air turbulence is an intermittent  
100 process: infrequent wind gusts sweeping downward through the trunk space from the air above are  
101 responsible for much of the exchange of heat, vapour and momentum between the canopy and the  
102 atmosphere. The 'effective diffusivity' of heat and vapour is more often a function of the vertical  
103 distribution of heat and water vapour sources or sinks within the canopy than of the turbulence level.  
104 Simulation of within-canopy turbulence is thus improved upon by using Lagrangian (e.g. Raupach,

105 1989) or Eulerian (e.g. Katul and Albertson, 1999) advection-diffusion models. The utility of such  
106 models for ecological applications, however, is severely limited by their need to specify length and time  
107 scales for the wind field. *K*-theory models are least valid when they are used to estimate within-canopy  
108 water vapour and heat exchange, but it is by virtue of this fact that it is still possible to simulate realistic  
109 in-canopy microclimates using *K*-theory. This apparent inconsistency arises for two reasons. First,  
110 although the source-sink strengths and hence the distribution of heat and momentum fluxes are  
111 extremely sensitive to the shape of measured profiles (Finnigan, 2000; Raupach and Thom, 1981), the  
112 converse relationship means that shape of the temperature and wind profiles are insensitive to flux  
113 uncertainties and can be generated by integration of an appropriate distribution of sources. Second, both  
114 temperature and humidity are related strongly to latent heat fluxes, which in turn are more strongly  
115 controlled by stomatal conductance than by turbulence within the canopy (Jarvis and McNaughton,  
116 1986). In consequence, a realistic representation of the distribution of foliage density, net radiation and  
117 stomatal conductance in various layers of a canopy, coupled with a relatively uncertain model of  
118 atmospheric transfer within the canopy, will tend to adequately reproduce temperature, vapour and wind  
119 profiles (Monteith and Unsworth, 2013).

120

121 Thus, despite evolving views of the processes driving turbulence within plant canopies, different models  
122 developed over several decades (e.g. Bailey et al., 2016; Baldocchi and Meyers, 1998; Goudriaan, 1977;  
123 McNaughton and Van den Hurk, 1995; Waggoner et al., 1969) have all used a similar approach. First,  
124 the vertical distribution of radiant energy within the canopy is quantified from foliage density and  
125 radiation transmission. Second, the net radiation absorbed by each leaf is divided up into sensible and  
126 latent heat, making appropriate assumptions about stomatal and leaf boundary layer conductance. Last,  
127 the transfer of air within different layers of the canopy is modelled using a variety of different  
128 approaches (e.g. *K*-theory, Lagrangian or Eulerian models) and have all been shown to perform in a  
129 similar fashion and relatively well (Bache, 1986; Dolman and Wallace, 1991). Nevertheless, a practical,  
130 ‘off-the-shelf’ model that can be used by ecologists to estimate microclimate conditions is still lacking.

131 Here we develop an integrated above/below-canopy and soil microclimate model, in the R programming  
132 environment, for application in ecological research. The model, based on first principles physics, is  
133 designed to be flexible, enabling application in almost any terrestrial environment though its intended  
134 focus is primarily to estimate within-canopy temperatures. Through its modular design, and careful  
135 selection of vegetation parameters typical of a given vegetation derived from literature, it can be applied  
136 with little knowledge of the particular study location (as a minimum, just a user-specified broad habitat  
137 type). However, the option to alter parameters (for example, stomatal conductance, or leaf area at  
138 varying heights in the canopy) is included to enable more complex, bespoke parametrisations where  
139 possible. The model can also be run using freely available climate data using tools that we have  
140 previously developed for downloading (Duffy, 2020; Kearney et al., 2020).

141

## 142 2. MODEL DESCRIPTION

### 143 2.1 Overall model structure

144 The model is designed to be run at single-point locations, using a time-series of climate forcing data  
145 (temperature, humidity, wind speed, atmospheric pressure and incoming solar radiation). It can be run  
146 in two modes at time-increments ranging from seconds to days. For application where very fine-  
147 temporal resolution data might be needed, heat and vapour exchange are modelled as transient  
148 processes, and heat storage by the canopy, and the exchange of heat between different layers of the  
149 canopy, are considered explicitly, with the capacity to simulate wind gusts thus bi-passing limitations  
150 associated with *K*-theory. Alternatively, for application at time increments of an hour or longer, below-  
151 canopy heat and vapour exchange are assumed to attain steady state, and the temperatures and soil  
152 moisture are determined using energy balance equations that sum to zero. In this latter mode, the model  
153 has been integrated with `NicheMapR` package (Kearney and Porter, 2017) and uses the rapid  
154 processing capacity of Fortran routines therein to compute soil moisture and temperature. It also enables  
155 explicit modelling of snow.

156 In the transient mode, the canopy and soil profiles are divided into a user-specified number of layers  
157 (with a default of 20). For each layer, the user specifies canopy properties (e.g. leaf area, leaf angle  
158 distribution, leaf reflectance and maximum stomatal conductance) and soil (e.g. bulk density, mineral,  
159 organic, quartz and clay content, Campbell 1985), or alternatively these are estimated for each layer by  
160 specifying habitat or soil type or providing single values for the entire canopy and soil profile. In the  
161 steady-state mode, the user specifies a height below ground or above/within the canopy, and the leaf  
162 area above this point and for the canopy in total must be specified (although the option to estimate these  
163 by specifying a habitat type is also included). In both modes, above-canopy temperature, humidity and  
164 wind profiles are calculated using *K*-theory with estimates of bulk aerodynamic resistance derived from  
165 canopy properties. Within the canopy, radiation transmission and wind profiles are also estimated from  
166 canopy properties. These, in turn, are used to estimate turbulent transfer within the canopy and boundary  
167 layer and stomatal conductance for each canopy layer. Heat balance equations for each canopy layer  
168 are then linearized, enabling simultaneous calculation of leaf and air temperatures. Time-dependent  
169 differential equations for each canopy and soil node are then specified and storage and simultaneous  
170 exchanges of heat and vapour between each layer then computed. In the transient mode, storage is  
171 considered both for soil and the canopy, but in the steady-state mode, only storage in the soil is  
172 considered. The model returns a time-series of temperature, humidity and wind speeds at user-specified  
173 heights or depths.

174 Below we provide a general overview of the equations used in the model. All symbols and their units  
 175 are described in Table 1, and further details of these equations and their derivation are provided in  
 176 Appendix A.

177

178 **Table 1.** List of symbols used in equations.

<b>Term</b>	<b>Definition</b>	<b>Units</b>
$a$	Wind attenuation coefficient	-
$b$	Exponent for water release from soil	-
$c_d$	Drag coefficient	-
$C_D$	Volumetric specific heat capacity of vegetation	$\text{J}\cdot\text{m}^{-3}\cdot\text{K}^{-1}$
$C_H$	Volumetric specific heat capacity of soil	$\text{J}\cdot\text{m}^{-3}\cdot\text{K}^{-1}$
$c_p$	Specific heat of air at constant pressure	$\text{J}\cdot\text{mol}^{-1}\cdot\text{K}^{-1}$
$d$	Zero plane displacement	m
$D_H$	Thermal diffusivity	$\text{m}^2\cdot\text{s}^{-1}$
$e$	Vapour pressure	Pa
$e_L$	Vapour pressure of leaf	Pa
$e_s$	Saturated vapour pressure	Pa
$E$	Evaporation rate of water	$\text{mol}\cdot\text{m}^{-2}\cdot\text{s}^{-1}$
$g$	Molar conductance	$\text{mol}\cdot\text{m}^{-2}\cdot\text{s}^{-1}$
$g_c$	Stomatal conductance	$\text{mol}\cdot\text{m}^{-2}\cdot\text{s}^{-1}$
$g_{cmx}$	Maximum stomatal conductance	$\text{mol}\cdot\text{m}^{-2}\cdot\text{s}^{-1}$
$g_{Ha}$	Leaf boundary layer conductance for heat	$\text{mol}\cdot\text{m}^{-2}\cdot\text{s}^{-1}$
$G_r$	Grashof number	-
$g_v$	Leaf conductance for vapour	$\text{mol}\cdot\text{m}^{-2}\cdot\text{s}^{-1}$
$g_t$	Conductance for heat by turbulent transfer	$\text{mol}\cdot\text{m}^{-2}\cdot\text{s}^{-1}$
$h$	Canopy height	m
$H$	Sensible heat flux density	$\text{W}\cdot\text{m}^{-2}$
$i_w$	Relative turbulence intensity	-
$l_m$	Mixing length	m
$l_{tr}$	Transmission fraction of longwave radiation through the canopy	-
$k$	Thermal conductivity	$\text{W}\cdot\text{m}^{-1}\cdot\text{K}^{-1}$
$K$	Extinction coefficient for canopy radiation transmission	-
$m_i$	Ratio of radiation incident on inclined leaves in each canopy layer relative to the horizontal	-
$n$	Thomas algorithm forward-backward weighting factor	-
$p_a$	Atmospheric pressure	Pa
$p_s$	Fraction of sunlit leaves	-
$P_{AI}$	Plant area index	-
$P_r$	Prandtl number	-
$P_v$	Fractional foliage volume	-
$Q_a$	Photosynthetically active radiation absorbed by a leaf	$\text{mol}\cdot\text{m}^{-2}\cdot\text{s}^{-1}$
$Q_{a50}$	Value of $Q_a$ when $g_v$ is at 50% of maximum	$\text{mol}\cdot\text{m}^{-2}\cdot\text{s}^{-1}$
$R_{abs}$	Total radiation absorbed by canopy layer	$\text{W}\cdot\text{m}^{-2}$
$R_{em}$	Total radiation emitted by canopy layer	$\text{W}\cdot\text{m}^{-2}$
$R_b^0$	Flux density of beam radiation on a horizontal surface above the canopy	$\text{W}\cdot\text{m}^{-2}$

Term	Definition	Units
$R_b^{PAI}$	Flux density of beam radiation below plant area $P_{AI}$	$W \cdot m^{-2}$
$R_d^0$	Flux density of diffuse radiation above the canopy	$W \cdot m^{-2}$
$R_d^{PAI}$	Flux density of diffuse radiation below plant area $P_{AI}$	$W \cdot m^{-2}$
$R_e$	Reynolds number	-
$r_l$	Leaf reflectivity (longwave radiation)	-
$R_l^{abs}$	Longwave radiation absorbed by canopy layer	$W \cdot m^{-2}$
$R_l^{can}$	Longwave radiation emitted by canopy to each layer	$W \cdot m^{-2}$
$R_l^{em}$	Emitted longwave radiation	$W \cdot m^{-2}$
$R_l^{sky}$	Longwave radiation emitted by sky	$W \cdot m^{-2}$
$r_s$	Leaf reflectivity (shortwave radiation)	-
$R_s^{abs}$	Shortwave radiation absorbed by canopy layer	$W \cdot m^{-2}$
$R_s^{PAI}$	Flux density of shortwave radiation below plant area $P_{AI}$	$W \cdot m^{-2}$
$t$	Time step	s
$T_{d+z_H}$	Temperature at heat exchange surface of canopy	K
$T_j$	Temperature at time $j$	K
$T_z$	Temperature at height $z$	K
$T_l$	Leaf temperature	K
$u^*$	Friction velocity of wind	$m \cdot s^{-1}$
$u_h$	Wind speed at top of canopy	$m \cdot s^{-1}$
$u_z$	Wind speed at height $z$	$m \cdot s^{-1}$
$V_d$	Volumetric density of vegetation	$kg \cdot m^{-3}$
$w$	Mean leaf width	m
$x$	Ratio of vertical to horizontal projections of a representative volume of foliage	
$x_d$	Characteristic dimension of leaf	m
$z$	Height	m
$Z$	Solar zenith angle	°
$z_H$	Roughness length for heat	m
$z_{LA}$	Mean leaf-air distance	m
$z_M$	Roughness length for momentum	m
$\lambda$	Latent heat of vaporization of water	$J \cdot mol^{-1}$
$\theta$	Volumetric soil moisture fraction	-
$\theta_s$	Saturated volumetric soil moisture fraction	-
$\hat{\rho}$	Molar density of air	$mol \cdot m^{-3}$
$\sigma$	Stefan-Boltzman constant	$W \cdot m^{-2} \cdot K^{-4}$
$\psi_e$	Air entry water potential	$J \cdot kg^{-1}$
$\psi_H$	Diabatic correction for heat	-
$\psi_M$	Diabatic correction for momentum	-
$\Omega$	Canopy clumping factor	-

179

180

## 2.2 Solar radiation

181 Radiation is the key source of heat within a canopy and has a major bearing on rates of  
182 evapotranspiration. The net radiation flux is determined by the balance of incoming shortwave radiation  
183 and emitted longwave radiation, a portion of the latter of which is also absorbed by leaves. Direct  
184 radiation is partitioned into direct (beam) and diffuse components, both of which are attenuated by the

185 canopy. Following Campbell (1986) and Campbell & Norman (2012), the flux density of beam radiation  
 186  $R_b^{PAI}$  under plant area  $P_{AI}$  is described as follows:

$$R_b^{PAI} = R_b^0 \left\{ (1 - \Omega) \exp \left( -\sqrt{1 - r_s} K P_{AI} \left( \frac{1}{1 - \Omega} \right) \right) + \Omega \right\} \quad (1a)$$

187 where  $R_b^0$  is the flux density of beam radiation on a horizontal surface above the canopy,  $r_s$  is the  
 188 reflectance of leaves to shortwave radiation,  $\Omega$  (scaled between 0 and 1) describes how clumped the  
 189 canopy is such that some radiation passes directly through canopy gaps.  $K$ , the extinction coefficient of  
 190 light, represents the area of shadow cast on a horizontal surface by the canopy divided by the plant area  
 191 of the canopy, and depends on the ratio of vertical to horizontal projections of a representative volume  
 192 of foliage,  $x$ :

$$K = \frac{\sqrt{x^2 + \tan^2 Z}}{1.774(x + 1.182)^{-0.733}}$$

194 where  $Z$  is the solar zenith angle. For diffuse radiation, the leaf angle distribution is unimportant, and  
 195 (1a) becomes

$$R_d^{PAI} = R_d^0 \left\{ (1 - \Omega) \exp \left( -\sqrt{1 - r_s} P_{AI} \left( \frac{1}{1 - \Omega} \right) \right) + \Omega \right\} \quad (1b)$$

196 where  $R_d^0$  is the flux density of diffuse radiation above the canopy,  $R_d^{PAI}$  is the flux density of below  
 197 plant area  $P_{AI}$ . The temperature of leaves is dependent on the amount of radiation absorbed. Assuming  
 198 the canopy to be made up of  $n$  layers, each with a plant area,  $P_{AI}[i]$ , such that  $P_{AI}$  represents the plant  
 199 area above any given layer, then the flux density of solar radiation absorbed ( $R_s^{abs}$ ) by each layer is

$$R_s^{abs} = P_{AI}[i] (1 - r_s) (p_s m_i R_s^{PAI} + (1 - p_s) R_s^{PAI}) \quad (2)$$

200  
 201 where  $R_s^{PAI}$  is the flux density of solar radiation below plant area  $P_{AI}$  given by  $R_b^{PAI} + R_d^{PAI}$  and  $p_s$  is the  
 202 fraction of sunlit leaves given by

$$p_s = (1 - \Omega) \left( \frac{1 - \exp \left( -\frac{K P_{AI}}{1 - \Omega} \right)}{P_{AI} K} \right) + \Omega$$

204 and  $m_i$  is the ratio of radiation incident on inclined leaves in each canopy layer relative to the horizontal,  
 205 which from Campbell (1990) is approximated as follows:

$$m_i = \exp[1.206x^{0.407} - 4.89 - (0.412x^{0.317} + 1.324) \log(90 - Z)]^{-1}$$

### 208 2.3 Longwave radiation



209 From the Stefan–Boltzman law, the flux density of longwave radiation emitted by vegetation,  $R_l^{em}$ , with  
 210 plant area  $P_{AI}[i]$  is

$$R_l^{em} = P_{AI}[i](1 - r_l)\sigma T_L^4 \quad (2a)$$

211 where  $r_l$  is reflectance to longwave radiation,  $\sigma$  is the Stefan-Boltzman constant and  $T_L$  is the  
 212 temperature of the leaf. A portion of emitted radiation is then reabsorbed. The absorbed longwave  
 213 radiation,  $R_l^{abs}$ , depends on sky emissivity and upwards and downwards transmission through the  
 214 canopy

$$R_l^{abs} = P_{AI}[i](1 - r_l)(R_l^{sky} + R_l^{can}) \quad (2b)$$

215 where  $R_l^{sky}$  is longwave radiation absorbed and re-emitted downward from the sky, given by  
 216  $R_l^{sky} = \varepsilon_s(l_{tr})^2 R_l^{em}$  and  $R_l^{can}$  is radiation absorbed and re-emitted downward from the canopy, given by  
 217  $R_l^{can} = (1 - l_{tr})R_l^{em}$ , where  $\varepsilon_s$  is sky emissivity and  $l_{tr}$  is transmission of longwave radiation through the  
 218 canopy given by  $l_{tr} = (1 - \Omega)\exp\left(-\sqrt{1 - r_l}P_{AI}\left(\frac{1}{1 - \Omega}\right)\right) + \Omega$ .

#### 219 2.4 Wind, conductance and temperature above-canopy

220 Wind profiles above the canopy dictate heat and vapour exchange between the canopy and air above it,  
 221 and therefore ultimately determine temperature and vapour profiles. It can generally be assumed that  
 222 radiative fluxes have a negligible effect on air temperature directly. However, the canopy itself acts as  
 223 a heat exchange surface, enabling exchange of heat with surrounding air via a process of eddy diffusion.  
 224 Following Campbell and Norman (2012) the wind profile is describe as follows:

$$u_z = \frac{u^*}{0.4} \ln \frac{z - d}{z_M} + \psi_M \quad (3)$$

225 where  $u_z$  is wind speed at height  $z$ ,  $d$  is the height above ground within the canopy where the wind  
 226 profile extrapolates to zero,  $z_m$  the roughness length for momentum,  $\psi_M$  is a diabatic correction for  
 227 momentum (see Appendix A) and  $u^*$  is the friction velocity, which gives the wind speed at height  $d +$   
 228  $z_m$ .

229 The equation that describes the temperature profile is given as follows:

$$T_z = T_{d+z_H} - \frac{H}{0.4\hat{\rho}c_p u^*} \left( \ln \frac{z - d}{z_H} + \psi_H \right) \quad (4)$$

230 where  $T_z$  is temperature at height  $z$ ,  $T_{d+z_H}$  is the temperature at the height of the exchange surface  $d +$   
 231  $z_H$ ,  $z_H$  is the roughness length for heat transfer,  $\psi_H$  the diabatic correction for heat and  $\hat{\rho}$  and  $c_p$  the  
 232 specific heat and molar density of air respectively. The sensible heat flux  $H$  is, in effect, the net heat  
 233 supplied to the canopy surface as determined from the balance of radiative, latent and ground heat  
 234 fluxes. Coefficients  $d$ ,  $z_M$  and  $z_H$  can be derived through empirical measurement of temperature and wind  
 235 profiles, but the model includes more general expressions of these derived by Shaw & Pereira (1982)

236 as functions  $P_{AI}$  and canopy height ( $h$ ). The diabatic correction factors account for the fact that strong  
 237 surface heating causes overturning of the air layers, with resultant increases in turbulence and mixing  
 238 and vis-versa. Further details of how these are calculated are provided in Appendix A.

239 Heat conductance,  $g_t$  ( $\text{mol} \cdot \text{m}^{-2} \cdot \text{s}^{-1}$ ) between any two heights  $z_1$  and  $z_0$  above-canopy, expressed in molar  
 240 form is then given by

$$g_t = \frac{0.4\hat{\rho}u^*}{\ln\left(\frac{z_1-d}{z_0-d}\right) + \psi_H} \quad (5)$$

## 241 2.5 Wind, and heat conductance below-canopy

242 From Inoue (1963), Cionco (1972) and Goudriaan (1977), a wind profile within the canopy can be  
 243 derived as follows:

$$u_z = u_h \exp\left(a\left(\frac{z}{h} - 1\right)\right) \quad (6)$$

244 where  $u_z$  is wind speed at height  $z$  within the canopy,  $u_h$  is wind speed at the top of the canopy at height  
 245  $h$ , and  $a$  is a wind attenuation coefficient given by  $a = \frac{c_d P_{AI} h}{2l_m i_w}$ , where  $c_d$  is a drag coefficient that varies  
 246 with leaf inclination and shape,  $i_w$  is a coefficient describing relative turbulence intensity and  $l_m$  is the  
 247 mean mixing length, equivalent to the free space between the leaves and stems. From Goudriaan (1977)

248  $l_m = \sqrt{\frac{4wh}{\pi P_{AI}}}$ , for vegetation that is long and narrow, or  $l_m = \sqrt[3]{\frac{6w^2h}{\pi P_{AI}}}$  for leaves shaped more like squares,  
 249 where  $w$  is the mean width of leaves and stems. Within-canopy heat conductance between any two  
 250 heights  $z_1$  and  $z_0$  below-canopy is then given by

$$g_t = \frac{u_h l_m i_w a}{\left(\exp\left(\frac{-az_0}{h-1}\right) - \exp\left(\frac{-az_1}{h-1}\right)\right) \psi_H} \quad (7)$$

251 where  $\psi_H$  is a within-canopy diabatic correction factor for heat (see Appendix A). It is also necessary  
 252 to calculate conductance,  $g_{Ha}$ , between the leaf and air. When wind speeds are moderate to high,  
 253 conduction is predominantly under laminar forced convection and from e.g. Campbell & Norman  
 254 (2012) is given by

$$g_{Ha} = \frac{0.664\hat{\rho}D_H R_e^{0.5} P_r^{0.5}}{x_d} \quad (8a)$$

255 where  $D_H$  is thermal diffusivity,  $x_d$  is the characteristic dimension of the leaf ( $x_d \approx 0.7w$ ),  $R_e$  is the  
 256 Reynolds number, and  $P_r$  is the Prandtl number. When wind speeds are low, an expression that is  
 257 adequate for leaves is given by (Campbell and Norman, 2012)

$$g_{Ha} = \frac{0.54\hat{\rho}D_H (G_r P_r)^{0.25}}{x_d} \quad (8b)$$

258 where  $G_r$  is the Grashof number. When the leaf is cooler than the air, the heat transfer is only half as  
 259 efficient so the constant 0.54 becomes 0.26. Equations (8a & b) describe conductance one would  
 260 measure under minimal turbulence. Based on measurements by Mitchell (1976), and following  
 261 Campbell & Norman (2012), turbulence is accounted for by using an enhancement factor of 1.4.  
 262 Formulae for computing the Reynolds, Prandtl and Grashof numbers are provided in Appendix A.

### 263 *2.6 Vapour and latent heat fluxes*

264 Vapour gradients control both evapotranspiration rates and latent heat fluxes and thus have a significant  
 265 bearing on temperature and humidity. From Fick's law, the transport of vapour is given by

$$\lambda E = g \frac{\partial e}{p_a} \quad (10)$$

266 where  $\lambda E$  is latent heat, comprising the latent heat of vapourization of water ( $\lambda$ ) and the evaporation  
 267 rate ( $E$ ),  $\partial e$  is the vapour pressure gradient and  $p_a$  is atmospheric pressure. For vapour exchange above  
 268 the canopy or between layers of air within the canopy, the conductance is the same as that for heat. The  
 269 conductance for vapour loss from leaves ( $g_v$ ), however, also depends on stomatal conductance ( $g_c$ )

$$270 \quad g_v = 1 / (1/g_{Ha} + 1/g_c)$$

271 Under ample root water supply, non-extreme temperatures and low humidity deficit,  $g_c$  varies through  
 272 the canopy only in response to variation in photosynthetically active radiation. The stomatal response  
 273 to the photosynthetically active radiation by an individual leaf ( $Q_i$ ), can be assumed (Kelliher et al.,  
 274 1995) to be given by a hyperbolic function:

$$g_c = \frac{Q_a}{Q_a + Q_{a50}} g_{cmx} \quad (11)$$

275 where  $g_{cmx}$  is maximum stomatal conductance and  $Q_{a50}$  is the value of  $Q_a$  when  $g_v = g_{vmx}/2$ . Körner  
 276 (1995) gives values of  $g_{cmx}$  for most major vegetation types in the world.

277 It can generally be assumed that the water potential of leaves is such that vapour concentration at the  
 278 evaporating surface is equal to the saturated vapour concentration at surface temperature, such that  $e_s$   
 279 can be determined from leaf temperature ( $T_L$ ). For the soil surface, an equivalent to vapour pressure  
 280 can, from Campbell & Norman (2012), be calculated as  $e_a = e_s \exp\left(\left(\theta/\theta_s\right)^{-b} (0.018\psi_e/8.31T_0)\right)$ ,  
 281 where  $e_s$  is calculated using soil surface temperature ( $T_0$ ),  $\theta$  is soil volumetric water content,  $\theta_s$  the  
 282 saturated water content,  $\psi_e$  the air entry water potential and  $b$  the exponent for water release. The  
 283 parameters  $\theta_s$ ,  $\psi_e$  and  $b$  depend on soil type, but are otherwise constant.

### 284 *2.7 Below-canopy temperature and humidity*

285 Under steady-state, the heat balance equation for the leaves in each canopy layer is as follows:

$$\bar{R}_{abs} - \bar{R}_{em} - \bar{H} - \bar{\lambda E} = \bar{R}_{abs} - \varepsilon_s \sigma \bar{T}_L^4 - c_p \bar{g}_{Ha} (\bar{T}_L - \bar{T}_A) - \lambda \bar{g}_v \frac{e_L - \bar{e}_a}{\bar{p}_a} = 0 \quad (12)$$

286 Where  $\bar{R}_{abs}$  is absorbed radiation,  $\bar{R}_{em}$  emitted radiation,  $\bar{H}$  the sensible heat flux,  $\bar{\lambda E}$  the latent heat  
 287 flux,  $\varepsilon_s$  the emissivity of the leaf,  $\sigma$  the Stefan-Boltzmann constant,  $\bar{T}_L$  the absolute temperature of the  
 288 leaf,  $\bar{T}_A$  the absolute temperature of the air surrounding the leaf,  $\lambda$  the latent heat of vaporisation of  
 289 water,  $e_L$  the effective vapour pressure of the leaf,  $\bar{e}_a$  the vapour pressure of air and  $\bar{p}_a$  atmospheric  
 290 pressure. Throughout, overbars denote a mean over the duration of the time-step.

291 A challenge in solving this equation is the dependency of latent heat and emitted radiation on leaf  
 292 temperature. The emitted radiation term can be solved readily by linearisation using binomial expansion  
 293 (see Appendix A). The latent heat term is usually solved algebraically through linearization using the  
 294 Penman-Monteith equation (Monteith, 1965; Penman, 1948), by assuming that air temperature  
 295 surrounding a leaf is closely coupled to the air above and uninfluenced by leaf temperature. We  
 296 explicitly consider the effects of leaf temperature on air temperature, and also the degree of coupling  
 297 with the soil and air above canopy. Defining a term,  $\Delta T_L$ , such that  $T_L = T_A - \Delta T_L$  and a linear  
 298 expression for air temperature such that  $T_A = a_A + b_A \Delta T_L$ , it can be shown (see Appendix A) that

$$299 \quad \Delta T_L = \frac{R_{abs} - a_R - a_L}{1 + b_R + b_L + b_H}$$

300 Where equations for each  $a$  and  $b$  term are provided in Table 2. Under transient conditions the heat  
 301 storage of each canopy layer is sufficient to prevent equilibrium. If superscript  $j$  denotes present time,  
 302 and  $j+1$  is one time-step in the future it can reasonably be assumed that e.g.  $\bar{T} = 0.5(T^j + T^{j+1})$ .  
 303 Defining  $m_L$  as the flux density required to heat a  $m^3$  of vegetation by one degree K, given by  
 304  $z_{LA} C_d V_d / t P_{AI}$ , where  $z_{LA}$  is the mean leaf-air distance (equivalent to half the average distance between  
 305 leaves),  $C_d$  the specific heat capacity of vegetation with volumetric density  $V_d$ ,  $t$  the duration of each  
 306 model time step and  $P_{AI}$  the total one-sided plant area per  $m^2$  ground area, an equivalent expression for  
 307 the transient leaf temperature change is given as follows:

$$T_L^{j+1} = T_L^j + \frac{\bar{R}_{abs} - a_R - a_H - a_L}{m_L (1 + b_R + b_H + b_L)} \quad (13)$$

308 Expressions for each  $a$  and  $b$  under transient conditions are also given in Table 2 and derivation of the  
 309 equation is in Appendix A.

## 310 2.8 Soil temperature

311 In the soil, heat storage is almost always significant, and Fourier's Law is combined with the continuity  
 312 equation to obtain a time dependent differential equation that describes soil temperature as a function  
 313 of depth and time:  $C_h \partial T / \partial t = \partial (k \partial T / \partial z) / \partial z$ , where  $C_h$  is volumetric specific heat and  $k$  thermal  
 314 conductivity in  $W \cdot m^{-1} K^{-1}$  ( $k = c_p \partial z g$ ), determined from soil properties and volumetric water content

315 (Appendix A). A closed-form solution to this time-dependent differential equation that extends beyond  
 316 simple sets of soil properties and boundary conditions is not possible. Following Campbell (1985), a  
 317 numerical solution is achieved by dividing the soil into layers. Each layer is assigned a node,  $i$ , at depth,  
 318  $z_i$ , and with heat storage,  $Ch_i$ , and nodes are numbered sequentially downward such that node  $i+1$   
 319 represents the node for the soil layer immediately below. Conductivity,  $k_i$ , represents conductivity  
 320 between nodes  $i$  and  $i+1$ . The energy balance equation for node  $i$  is then given by

$$\bar{\kappa}_i(\bar{T}_{i+1} - \bar{T}_i) - \bar{\kappa}_{i-1}(\bar{T}_i - \bar{T}_{i-1}) = \frac{C_{h_i}(T_i^{j+1} - T_i^j)(z_{i+1} - z_{i-1})}{2\Delta t} \quad (14)$$

321 where  $\Delta t$  is the time increment, conductance,  $\kappa_i = k_i/(z_{i+1} - z_i)$ , superscript  $j$  indicates the time at  
 322 which temperature is determined and overbars indicate means during the time increment.

### 323 2.9 Within-canopy heat and vapour exchange

324 Under transient conditions, the approach described for soil can readily be extended to account for the  
 325 exchange of heat between different layers of the canopy, with two notable exceptions. First, heat storage  
 326 in the air is substantially lower than in the soil and prior to computing heat exchange between layers,  
 327 air layers are merged when the total flux over the time increment exceeds heat capacity. Second, the  
 328 latent and sensible heat fluxes from the leaf to the air are also considered

$$\bar{g}_{Ha}c_p(\bar{T}_L - \bar{T}_i) + \frac{\lambda\bar{g}_v}{\bar{p}_a}(\bar{e}_L - \bar{e}_a) + \bar{g}_i c_p(\bar{T}_{i+1} - \bar{T}_i) - \bar{g}_{i-1}c_p(\bar{T}_i - \bar{T}_{i-1}) = \frac{c_p\bar{\rho}(1 - P_v)(T_i^{j+1} - T_i^j)(z_{i+1} - z_{i-1})}{2\Delta t} \quad (15)$$

329 where  $g_i$  is the molar conductance between canopy layers (7) and  $P_v$  is the fractional foliage volume  
 330 given by  $V_t[i]P_{AI}[i]/z_t[i]$ , where  $V_t[i]$  is the mean thickness of foliage and  $z_t[i]$  the thickness of each  
 331 canopy layer  $i$ .

332 The system of equations for each canopy layer can be combined with those for the soil layers to form a  
 333 single set of equations. Assuming  $\bar{T} = nT^{j+1} + (1 - n)T^j$ , where  $n$  is a weighting factor in the range  
 334 0 to 1. Equations (14) and (15) can be re-arranged and solved for  $T^{j+1}$  by Gaussian elimination using  
 335 the Thomas algorithm (Thomas, 1949), when boundary conditions are used to reduce the number of  
 336 unknowns by two. The upper boundary condition is the conductance  $\bar{g}_0$  between the top of the canopy  
 337 and the air at reference height determined from (5). A boundary condition at the bottom of the soil  
 338 profile is set by assuming that temperatures are stable and, in the absence of a user-provided value,  
 339 equivalent to mean air temperature over the duration the model is run.

340 Vapour exchange can be handled in a similar way, expect that here, water exchange in the soil is user-  
 341 specified, or in the steady-state mode, calculated using NicheMapR (see running the model) and the  
 342 exchange between air layers is given by

$$\frac{\bar{g}_v}{p_a}(\bar{e}_L - \bar{e}_a) + \frac{\bar{g}_i}{p_a}(\bar{e}_{i+1} - \bar{e}_i) - \bar{g}_{i-1}c_p(\bar{e}_i - \bar{e}_{i-1}) = \frac{\hat{\rho}(1 - P_v)(e_i^{j+1} - e_i^j)(z_{i+1} - z_{i-1})}{2\Delta t} \quad (16)$$

343 Again, the system of equations is solved by Gaussian elimination using the Thomas algorithm (see  
344 Appendix A).

345

### 346 3. RUNNING THE MODEL

347 The model is split into two R packages. The package ``microctools`` contains a series of ``worker``  
348 functions needed to run the model, such as those needed to compute conductance and radiation  
349 transmission. It also contains useful functions not directly needed to run the model, such as for  
350 estimating the diffuse fraction of total incoming solar radiation and converting between different  
351 humidity measures. The ``microclimc`` package contains the higher-level functions needed to compute  
352 individual elements of microclimate (for example leaf temperature), to run the model in its entirety over  
353 a single time increment (returning the full suite of microclimate variables for all layers in the canopy),  
354 or to run the model for a time-series to return temperature, humidity and wind speed at user-specified  
355 heights above or below ground. Package ``microctools`` is automatically installed when installing  
356 ``microclimc`` and is available on Github: <https://github.com/ilyamaclean/microclimc>.

357 There are two model run modes. Function ``runmodel`` runs the full model in transient mode, but in this  
358 mode, there are checks to establish whether conditions are steady state or transient, and the model  
359 automatically performs calculations accordingly. Function ``runmodels`` runs the model in steady-state  
360 mode for cases in which predictions for a single height is desired. However, it is encouraged to conduct  
361 steady state modelling using the wrapper function ``runwithNMR``, which invokes the ``NicheMapR``  
362 package to calculate soil moisture from rainfall and evapotranspiration. In alternative modes, soil  
363 moisture must be specified by the user.

364 Two sets of parameters are needed to drive the model: (1) vegetation parameters, describing canopy  
365 properties for multiple layers within the canopy and (2) soil parameters, enabling heat capacity and  
366 conductances within the soil to be calculated. However, a key goal in the development of this model is  
367 to enable estimates of microclimate with varying amounts of information available. The ``microctools``  
368 package therefore includes functions that will reproduce reasonable approximations of soil properties  
369 simply by specifying a soil type and seasonal variation in and the vertical distribution of foliage and  
370 leaf angles from habitat types. Alternatively, where multi-layer information on foliage is available, such  
371 as might be derived using a plant canopy analyser or from a series of digital hemispherical photographs  
372 taken at different heights in the canopy (see e.g. Thimonier et al., 2010), these data can be used instead.

373  
374

**Table 2.** Full equations for terms in equation 13 used to simultaneously estimate leaf and air temperatures. Terms are defined in Table 1. Overbars denote means during the time increment. Definitions for both steady-state and transient heat exchange are provided. Derivation of the equations is provided in Appendix A.

Steady-state	Transient
$a_E = \frac{\bar{g}_{tR}\bar{e}_R + \bar{g}_{t0}\bar{e}_0 + \bar{g}_v e_s[\bar{T}_R]}{\bar{g}_{tR} + \bar{g}_{t0} + \bar{g}_v}$	$a_E = \frac{\frac{0.5t\bar{g}_v}{z_{LA}} \Delta_V [T_L^j] \Delta T_L}{1 + 0.5t \left( \frac{\bar{g}_{tR}}{z_R - z_i} + \frac{\bar{g}_{t0}}{z_i} + \frac{\bar{g}_v}{z_{LA}} \right)}$
$b_E = \frac{\Delta_V [\bar{T}_R]}{\bar{g}_{tR} + \bar{g}_{t0} + \bar{g}_v}$	$b_E = \frac{\frac{0.5t\bar{g}_v}{z_{LA}} \Delta_V [T_L^j] \Delta T_L}{1 + 0.5t \left( \frac{\bar{g}_{tR}}{z_R - z_i} + \frac{\bar{g}_{t0}}{z_i} + \frac{\bar{g}_v}{z_{LA}} \right)}$
$a_R = \varepsilon_s \sigma a_A^4$	$a_R = \varepsilon_s \sigma T_L^{j4}$
$b_R = 4\varepsilon_s \sigma (a_A^3 b_A + \bar{T}_R^3)$	$b_R = \varepsilon_s \sigma 2T_L^{j3}$
$a_H = 0$	$a_H = c_p \bar{g}_{Ha} (T_L^j - a_A)$
$b_H = c_p \bar{g}_{Ha}$	$b_H c_p \bar{g}_{Ha} (0.5 - 0.5b_A)$
$a_L = \frac{\lambda \bar{g}_v}{\bar{p}_a} (e_s[\bar{T}_R] - a_e)$	$a_L = \frac{\lambda \bar{g}_v}{\bar{p}_a} (e_s[T_L^j] - a_e)$
$b_L = \frac{\lambda \bar{g}_v}{\bar{p}_a} (\Delta_V [\bar{T}_R] - b_E)$	$b_L = \frac{\lambda \bar{g}_v}{\bar{p}_a} (0.5\Delta_V [T_L^j] - b_E)$
$a_A = \frac{\bar{g}_{tR}\bar{T}_R + \bar{g}_{t0}\bar{T}_0}{\bar{g}_{tR} + \bar{g}_{t0}}$	$a_A = \frac{T_a^j + \frac{0.5}{m_a} \left\{ \frac{\bar{g}_{tR}}{z_R - z_i} \bar{T}_R + \frac{\bar{g}_{t0}}{z_i} \bar{T}_0 + \frac{\bar{g}_{Ha}}{z_{LA}} T_L^j + \frac{\lambda \bar{g}_v}{z_{LA} \bar{p}_a} (e_L^j + 0.5e_s[T_L^j]) - \frac{\lambda \bar{g}_v}{z_{LA} \bar{p}_a} a_E + \frac{\lambda \bar{g}_{t0}}{z_i \bar{p}_a} \bar{e}_0 - \frac{\lambda \bar{g}_{t0}}{z_i \bar{p}_a} a_E \right\}}{1 + \frac{0.5}{m_a} \left( \frac{\lambda \bar{g}_{t0}}{z_i \bar{p}_a} + \frac{\bar{g}_{t0}}{z_i} + \frac{\bar{g}_{Ha}}{z_{LA}} \right)}$
$b_A = \frac{\bar{g}_{Ha}}{\bar{g}_{tR} + \bar{g}_{t0}}$	$b_A = \frac{\frac{0.5}{m_a} \left\{ 0.5 \frac{\bar{g}_{Ha}}{z_{LA}} + \frac{\lambda \bar{g}_v}{z_{LA} \bar{p}_a} (0.5\Delta_V [T_L^j] - b_E) + \frac{\lambda \bar{g}_{t0}}{z_i \bar{p}_a} b_E \right\}}{1 + \frac{0.5}{m_a} \left( \frac{\lambda \bar{g}_{t0}}{z_i \bar{p}_a} + \frac{\bar{g}_{t0}}{z_i} + \frac{\bar{g}_{Ha}}{z_{LA}} \right)}, \text{ where } m_a = c_p \hat{\rho} (1 - V_d) / t P_{AI}$

375

376 A similar ethos is used with regards to input weather data. The standard input is a data file of  
377 temperature, humidity, wind speed, air pressure, sky emissivity and incoming solar radiation, but where  
378 one or more of these variables are unavailable, we point the users to options for retrieving them. The R  
379 package `microclima` (Kearney et al., 2020; Maclean et al., 2019) contains functions for downloading,  
380 and interpolating to hourly, the required climate data from the NOAA-NCEP reanalyses programme  
381 (Kanamitsu et al., 2002). Similarly, the R-package `mcera5` (Duffy, 2020) contains similar functions  
382 for retrieving data from the ECMWF ERA5 reanalysis programme (Hersbach, 2016). Full instructions  
383 for running the model are available as a vignette included with the package, provided in Appendix B.  
384 The model can be run in time-steps ranging from one second to daily, with the time-increment controlled  
385 by the climate forcing data provided.

#### 386 **4. MODEL VALIDATION**

387 Both steady-state and transient modes of the model were validated using hourly empirical temperature  
388 measurements from four sites representing temperate deciduous and coniferous forests (Table 3; Lee et  
389 al., 1999; Munger and Hadley 2020; Templer et al., 2019; Teramoto et al., 2019)). Only validation data  
390 sampled according to best practices for micrometeorological observation (i.e. use of ultrafine-wire  
391 thermocouples; de Podesta et al., 2018; Rebmann et al., 2018) were used. Heights at which temperature  
392 was measured varied between sites (between 1.0 and 10.0 metres) but were always below the uppermost  
393 layers of the forest canopy; predictions were made for the same heights as measurements. The model  
394 was parameterized using biome-specific estimates of vegetation and soil profile parameters that are  
395 built into the package (see package details and vignette in Appendix B for details and the full list of  
396 parameters and default estimates).

397 We provided ERA5 hourly reanalysis data (Hersbach, 2016) as reference macroclimate and climate  
398 forcing to the microclimate model, corresponding to the times and points modelled. For the steady-state  
399 mode, daily resolution NCEP-DOE Reanalysis II precipitation estimates were provided for the soil  
400 moisture module (Kanamitsu et al. 2002). Because proper handling of snow cover and sub-freezing  
401 temperatures in the model is still under active development for the transient model, we constricted input  
402 data and predictions to only spring, summer and autumn months. For the purposes of this manuscript  
403 only air temperature predictions are validated (Figs. 1 and 2).

404 In the steady-state mode of the model, calculations are conducted simultaneously for all temporal  
405 timesteps, and therefore running the model for one year of data took an average of 5.28 seconds (on a  
406 single 2.2 GHz Intel i7 core with 4.0 GB of total memory). The transient mode, accessed via the function  
407 `runmodel`, must be run in sequence for each timestep, and so took an average of 194.9 seconds for the  
408 same time period. The steady-state and transient mode predicted below-canopy temperatures with  
409 similar accuracy (Mean absolute error 2.77 (transient) and 2.79 (steady-state); root mean square error



410 3.48 (both); 80.0% of variance explained (transient) and 79% (steady-state); Table 4). It should be noted  
411 that some of the error is likely due to errors associated with climate data used to drive the models.

412 Below-canopy temperatures were typically less variable than macroclimate temperatures, which was  
413 generally captured by the model in both of its modes. Both the steady-state and transient model  
414 underestimated forest temperature to a moderate degree (empirical SD: 5.93; steady-state estimate SD:  
415 5.44; transient estimate SD: 4.67). At the Fuji Hokuroku and Hubbard Brook site there is also evidence  
416 of a fairly consistent over-estimation of temperatures. This may in part be attributable to altitudinal  
417 differences between validation sites and the coarse-resolution ERA5 data, which differ on average by  
418 111 meters from the mean elevation across the ~25-kilometre ERA5 grid cells. For the purpose of  
419 reproducibility by users, and so as to provide a conservative estimate of model performance, we did not  
420 attempt to correct for these elevation differences.

421

## 422 **5. MICROCLIMATE PROFILES**

### 423 *5.1 Thermal Profiles*

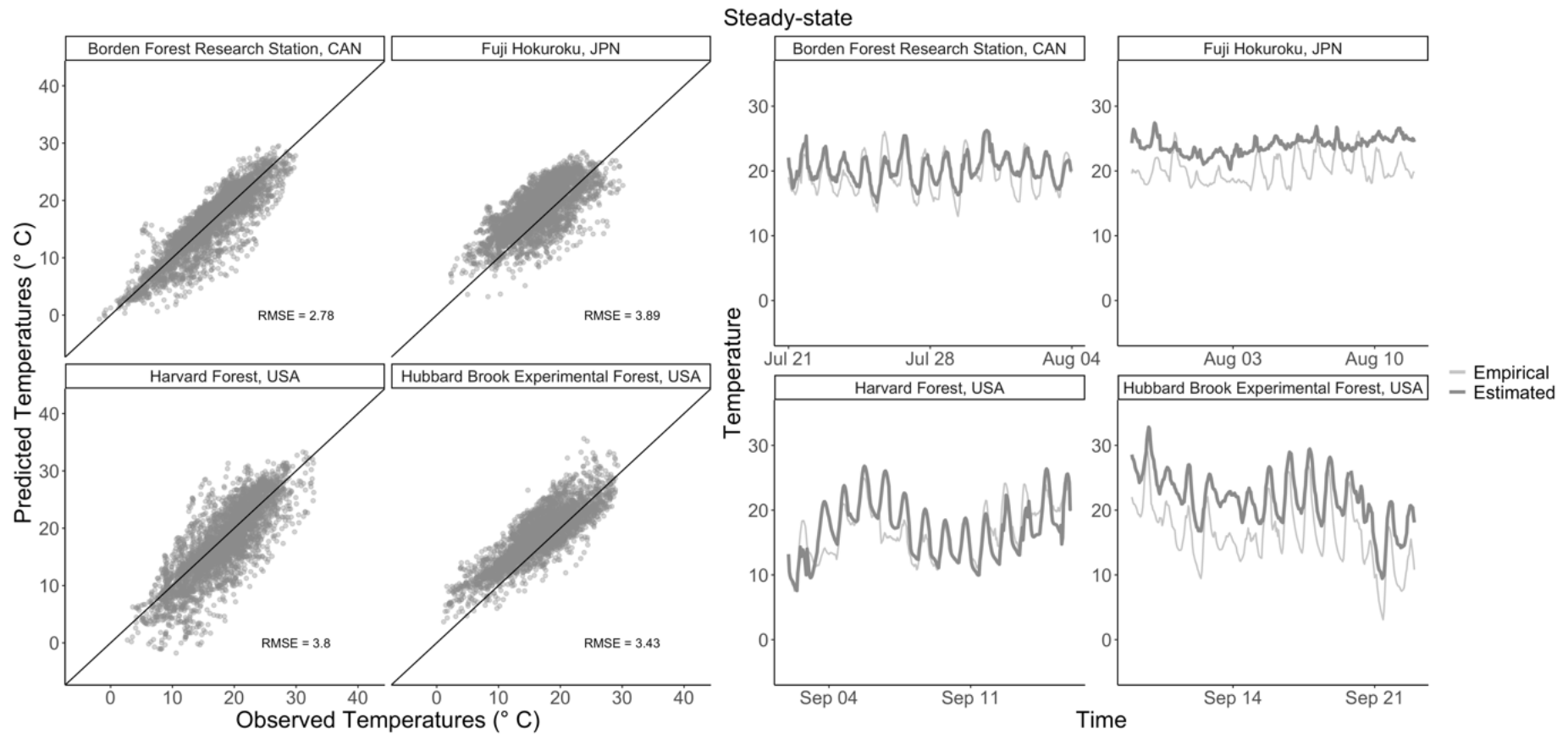
424 Typical profiles obtained by the model are shown in Figures 3 and 4 and highlight the magnitude of  
425 differences in climatic conditions within the soil and above or below canopy. Here temperature and  
426 humidity profiles were predicted for a location in Cornwall, United Kingdom (50.2178°N, 5.32656°W)  
427 for a deciduous forest (Fig. 3) and short grassland (Fig. 4). In both instances, vegetation parameters  
428 were derived automatically by specifying a habitat type. In forest, under both dry and humid warm  
429 daytime conditions, air temperature averaged over one hour were predicted to have a maximum in mid-  
430 canopy. These findings are consistent with those of other studies (e.g. Finnigan, 2000), and indicative  
431 of a zone of high radiation absorption associated with high foliage density and reduced heat exchange  
432 with air above-canopy caused by greater distance and reduced wind speed. In contrast, leaf temperatures  
433 were predicted to be highest near the top of the canopy, where self-shading is lowest. At night, leaf  
434 temperatures are lowest near the top of the canopy, particularly under clear-sky conditions. Here a lower  
435 proportion of the radiation emitted by a leaf would be expected to be absorbed and re-emitted by the  
436 canopy. In contrast, differences in canopy air temperatures were predicted to be modest. The cooling  
437 effect of leaves is offset by greater heat exchange with air above the canopy. The relative humidity  
438 profile reflects three factors. On the one hand, relative humidity would be expected to be lowest where  
439 temperatures are higher, as for a given vapour pressure relative humidity is primarily a function of  
440 temperature. However, evapotranspiration from leaves and vapour exchange with air above the canopy  
441 are also important. Despite limitations in the extent to which *K*-theory accurately captures canopy  
442 turbulence, the predicted wind profiles are remarkably similar to empirically-derived profiles reported  
443 in other studies (e.g. Raupach and Thom, 1981).

444

445 **Table 3.** Descriptions of sites and empirical temperature measurements used for model validation.

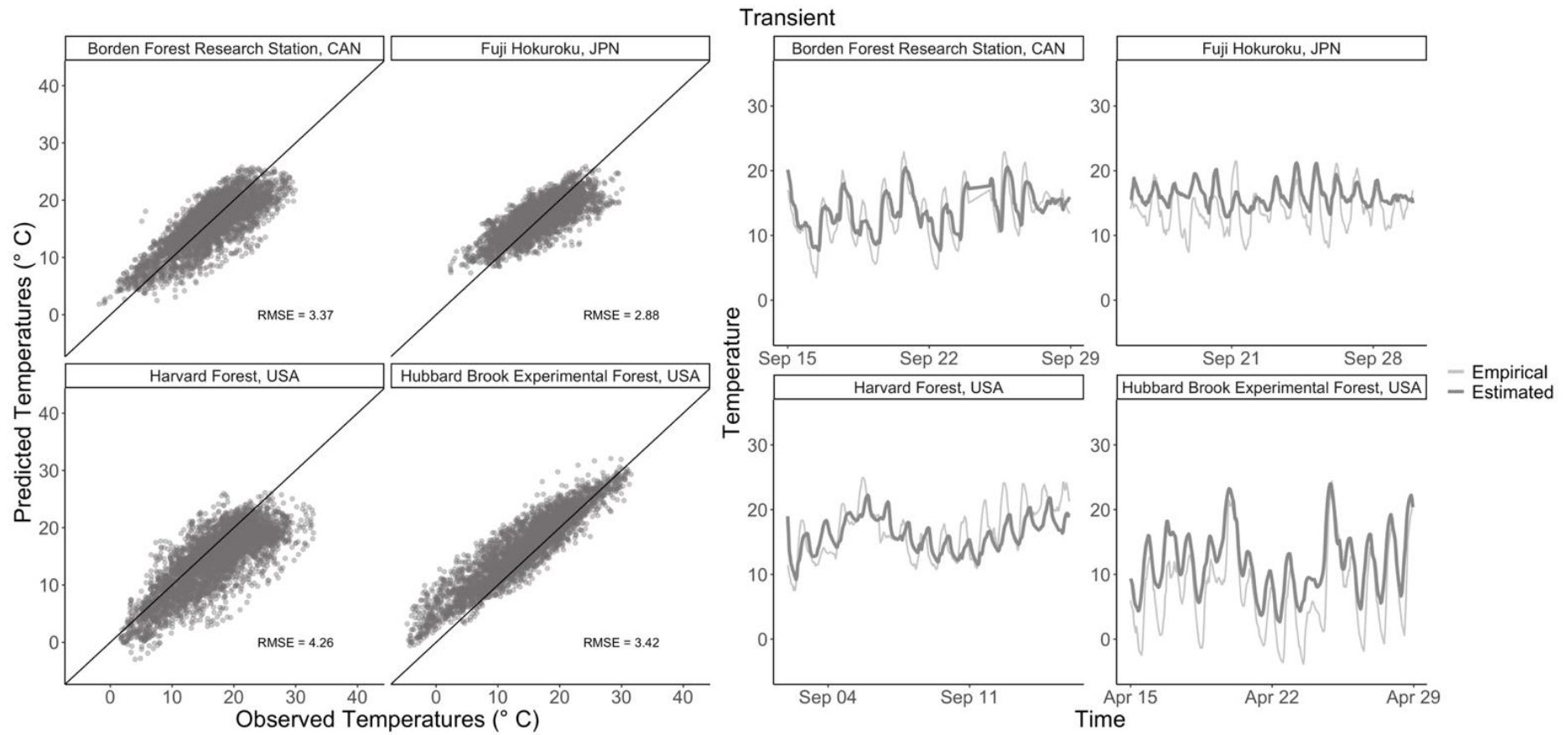
<b>Name</b>	<b>Latitude, Longitude</b>	<b>Vegetation</b>	<b>Temperature sensor</b>	<b>Measurement height (m)</b>	<b>Time start</b>	<b>Time end</b>
Borden Forest Research Station, Ontario, Canada	44°19'N, 79°56'W	Mixed hardwood/coniferous forest dominated by red maple and eastern white pine, 22 m canopy height	Aspirated copper–constantan thermocouples	1.7	1/04/1998	29/10/1998
Harvard Forest Hemlock Tower, Massachusetts, United States	42°32'N, 72°11'W	Hemlock-dominated temperate forest with mixed maple, oak, and pine, 23 m canopy height	Campbell Scientific CS215 sensor with aspirated radiation shield	1	4/04/2017	31/10/2017
Fuji Hokuoku Flux Observation Site, Yamanashi, Japan	35°27'N, 138°46'W	Deciduous and evergreen needleleaf forest, predominantly Japanese larch. 23 m canopy height	Vaisala HMP45A, platinum resistance thermometer	10	3/05/2019	30/09/2019
Hubbard Brook Experimental Forest	43°57'N, 71°42'W	Red maple-dominated mixed temperate forest, 22 m canopy height	Campbell Scientific CS215 sensor with aspirated radiation shield	6	1/04/2013	30/09/2013

446



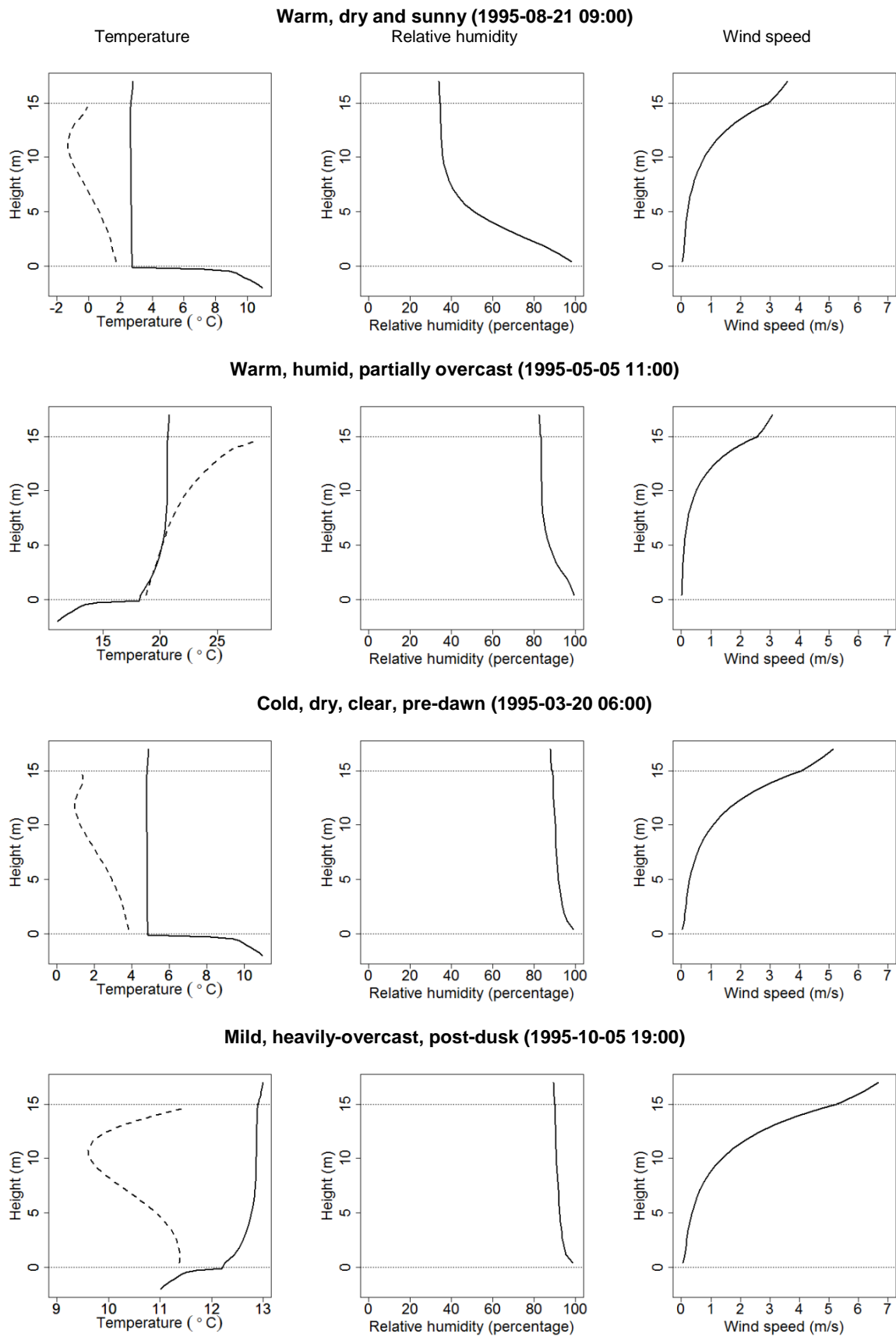
448

449 **Fig. 1.** Steady-state model predictions of temperature plotted across empirical measurements at four forested sites. Measurements were taken at heights ranging  
 450 from 1.0 m to 10.0, but all below the uppermost layers of canopy. Both thermal measurements and predictions were taken at hourly time-steps for 5-7 months  
 451 per site, and here subsets of time series are plotted to demonstrate diel variability.

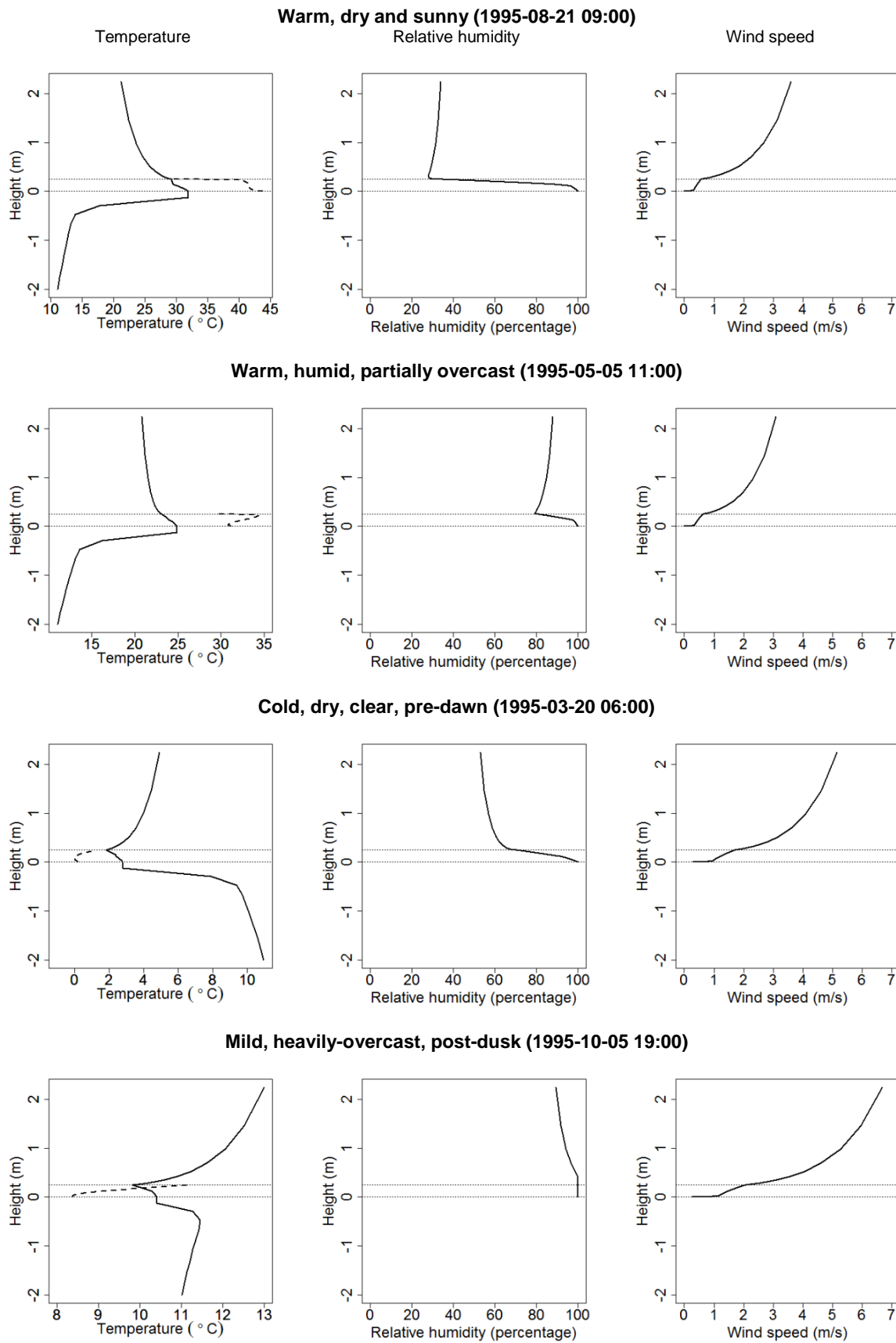


452

453 **Fig. 2.** Transient model predictions of temperature plotted across empirical measurements at four forested sites. Transient predictions had moderately lower  
 454 error than steady-state predictions (fig. 1), although the model did not accurately predict temperatures near freezing.



455 **Fig 3.** Modelled temperature (left), relative humidity (middle) and wind profiles (right) above, below  
 456 and within a 15 m tall deciduous forest canopy on four days with contrasting weather conditions. Dotted  
 457 lines in temperature profiles represent leaf temperatures, solid lines air temperature



458 **Fig 4.** Modelled temperature (left), relative humidity (middle) and wind profiles (right) above, below  
 459 and within a 25 cm height grassland on four days with contrasting weather conditions. Dotted lines in  
 460 temperature profiles represent leaf temperatures, solid lines air temperature

461 **Table 4.** Microclimate model average performance in steady-state and transient modes. Mean absolute  
 462 error, root mean square error, and Pearson’s correlation coefficients reported are relative to the  
 463 empirical temperature measurements.

Variable	Steady-State	Transient
Avg. run time (1 year timeseries)	5.28 s	187.80 s
MAE	3.3	2.77
RMSE	4.15	3.48
$r^2$	0.803	0.8

464

465 In the grassland, particularly in sunny conditions, air temperature decreases with height above-canopy  
 466 and is highest at points near the top of the canopy. Temperatures in the soil decrease with depth. At  
 467 night, under cold, clear-sky conditions when air temperature is lower than that of the deepest soil layer,  
 468 the profile is reversed. Under overcast conditions, when air temperatures are similar to ground  
 469 temperatures, variation in temperature with height is minimal, though there is a distinct zone close to  
 470 the soil surface where temperatures are lower. Leaf temperature profiles are broadly similar to air  
 471 temperature profiles within the canopy. As with deciduous forest, relative humidity profiles partially  
 472 reflect the temperature profiles, being lowest where temperatures are higher. However, is noticeable  
 473 that during dry sunny conditions relative humidity is highest within the vegetation itself, despite warmer  
 474 temperatures, reflecting the zone of evapotranspiration. Wind profiles are typical of those empirically  
 475 observed (Campbell and Norman, 2012), and, though partially affected by diabatic turbulence, are  
 476 broadly consistent irrespective of conditions.

477

478 **6. CONCLUDING REMARKS**

479 Our model, written for the R programming environment, complements existing R packages for  
 480 modelling microclimate (Kearney and Porter, 2017; Maclean et al., 2019), but extends the utility of  
 481 these packages by enabling ecologists to predict adequately the microclimate above, within, and below  
 482 dense canopies, such as those of forests. Since many organisms live in forest environments, this is likely  
 483 to be particularly useful. A key goal in developing our model was to enable estimates of microclimate  
 484 with varying amounts of information available. In consequence, default parameters drawn from  
 485 literature are provided for broad habitat and soil types, but in circumstances where more detailed site-  
 486 specific information, this can be readily incorporated. Estimates of snow cover and its effects on  
 487 temperature can be accounted for by invoking the snow subroutine within the `NicheMapR` package,  
 488 which builds nodes of snow above the surface conditional on the amount of precipitation, and thereby  
 489 influencing albedo and surface-air heat exchange. Accounting for snow would be especially valuable  
 490 for improved predictions near freezing, a current limitation of our model. Predictions of below-canopy  
 491 soil temperatures are currently provided by the model, yet these are primarily to estimate heat exchange

492 with the air. Accurate soil temperature predictions are contingent upon capturing dynamic soil moisture,  
493 which in the steady-state mode can be achieved via integration with `NicheMapR`.

494 Time series of sub-canopy temperatures from four forest locations globally are used to test the model.  
495 The results indicate that temperatures can be estimate with a moderate degree of accuracy. A degree of  
496 error is to be expected, however, as the climate forcing datasets used to drive the model are themselves  
497 imperfect and used we used default vegetation parameters associated with the broad habitat types of  
498 these sites rather than quantifying vegetation structure *in situ*. Improvements in model fit would be  
499 expected with finer-tuning of model parameters to account for local conditions and by correcting the  
500 climate forcing data, for example by accounting for elevation effects (see e.g. Maclean *et al.* 2019).  
501 Nevertheless, even without doing so, the mean error of temperature measurements is only in the order  
502 of 2.5-3°C.

503 Though there are still uncertainties in understanding of the microclimatic processes operating below  
504 canopy, many of the fundamental principles of microclimate modelling have been resolved decades.  
505 However, few of these insights have diffused into the field of ecology and the lack of integration  
506 between ecology and micrometeorology is perhaps one of the most remarkable examples of a  
507 disciplinary division. While many of the principles of microclimate modelling were resolved decades  
508 ago, in the very situations in which such models are much needed, they are rarely utilised. Here we  
509 utilised principles of environmental physics to provide a step forward in bridging this gap.

510

## 511 **Acknowledgements**

512 The work was supported by the Met Office Hadley Centre Climate Programme (HCCP) funded by BEIS  
513 and Defra through collaboration with Dr Deborah Hemming, who leads HCCP work on UK pest risk  
514 with Defra's Animal and Plant Health Team. Additional support was provided by the European Regional  
515 Development Fund Agri-tech Cornwall Programme. DK was supported by the National Science  
516 Foundation Graduate Research Fellowship Program (No. 2019277511). We thank anonymous referees  
517 for helpful comments and Katie Thurston for proof-reading the manuscript.

518

## 519 **References**

- 520 Ali, H.B., Bournet, P.-E., Cannavo, P., Chantoiseau, E., 2018. Development of a CFD crop submodel  
521 for simulating microclimate and transpiration of ornamental plants grown in a greenhouse under  
522 water restriction. *Computers and Electronics in Agriculture* 149, 26-40.
- 523 Bache, D., 1986. Momentum transfer to plant canopies: Influence of structure and variable drag.  
524 *Atmospheric Environment* 20, 1369-1378.



525 Bailey, B.N., Stoll, R., Pardyjak, E.R., Miller, N.E., 2016. A new three-dimensional energy balance  
526 model for complex plant canopy geometries: Model development and improved validation  
527 strategies. *Agricultural and Forest Meteorology* 218, 146-160.

528 Baker, C., 1980. Some Problems in Using Meteorological Data to Forecast the Timing of Insect Life  
529 Cycles 1: Problèmes rencontrés dans L'utilisation des données météorologiques pour prévoir le cycle  
530 évolutif des insectes. *EPPO Bulletin* 10, 83-91.

531 Baldocchi, D., Meyers, T., 1998. On using eco-physiological, micrometeorological and biogeochemical  
532 theory to evaluate carbon dioxide, water vapor and trace gas fluxes over vegetation: a perspective.  
533 *Agricultural and Forest Meteorology* 90, 1-25.

534 Banerjee, T., De Roo, F., Mauder M. (2017) Connecting the Failure of *K* Theory inside and above  
535 Vegetation Canopies and Ejection-Sweep Cycles by a Large-Eddy Simulation. *Journal of Applied*  
536 *Meteorology And Climatology*, 56, 3119-3131.

537 Bennie, J., Huntley, B., Wiltshire, A., Hill, M.O., Baxter, R., 2008. Slope, aspect and climate: spatially  
538 explicit and implicit models of topographic microclimate in chalk grassland. *Ecological Modelling*  
539 216, 47-59.

540 Bramer, I., Anderson, B.J., Bennie, J., Bladon, A.J., De Frenne, P., Hemming, D., Hill, R.A., Kearney,  
541 M.R., Körner, C., Korstjens, A.H., 2018. Advances in monitoring and modelling climate at  
542 ecologically relevant scales. *Advances in Ecological Research* 58, 101-161.

543 Bruse, M., 2014. ENVI-Met 4. <http://www.envi-met.info>.

544 Buckley, L.B., Cannistra, A.F., John, A., 2018. Leveraging organismal biology to forecast the effects  
545 of climate change. *Integrative and Comparative Biology* 58, 38-51.

546 Campbell, G., 1990. Derivation of an angle density function for canopies with ellipsoidal leaf angle  
547 distributions. *Agricultural and forest meteorology* 49, 173-176.

548 Campbell, G.S., 1985. *Soil physics with BASIC: transport models for soil-plant systems*. Elsevier.

549 Campbell, G.S., 1986. Extinction coefficients for radiation in plant canopies calculated using an  
550 ellipsoidal inclination angle distribution. *Agricultural and forest meteorology* 36, 317-321.

551 Campbell, G.S., Norman, J., 2012. *An introduction to environmental biophysics*. Springer Science &  
552 Business Media.

553 Cionco, R.M., 1972. A wind-profile index for canopy flow. *Boundary-Layer Meteorology* 3, 255-263.

554 Curtis, E.M., Knight, C.A., Leigh, A., 2019. Intracanopy adjustment of leaf-level thermal tolerance is  
555 associated with microclimatic variation across the canopy of a desert tree (*Acacia papyrocarpa*).  
556 *Oecologia* 189, 37-46.

557 de Podesta, M., Bell, S., Underwood, R., 2018. Air temperature sensors: dependence of radiative errors  
558 on sensor diameter in precision metrology and meteorology. *Metrologia* 55, 229-244.

559 Dolman, A., Wallace, J., 1991. Lagrangian and K-theory approaches in modelling evaporation from  
560 sparse canopies. *Quarterly Journal of the Royal Meteorological Society* 117, 1325-1340.

561 Duffy JP, 2020. R package mcera5. Tools to Acquire and Process ERA5 Data for use in Microclimate  
562 Modelling. Available: <https://github.com/everydayduffy/mcera5>.

563 Evans, M.R., 2012. Modelling ecological systems in a changing world. *Philosophical Transactions of*  
564 *the Royal Society B: Biological Sciences* 367, 181-190.

565 Fick, S.E., Hijmans, R.J., 2017. WorldClim 2: new 1-km spatial resolution climate surfaces for global  
566 land areas. *International Journal of Climatology* 37, 4302-4315.

567 Finnigan, J., 2000. Turbulence in plant canopies. *Annual review of fluid mechanics* 32, 519-571.

568 Gardner, A.S., Maclean, I.M., Gaston, K.J., 2020. A new system to classify global climate zones based  
569 on plant physiology and using high temporal resolution climate data. *Journal of Biogeography*.

570 Gardner, T.A., Barlow, J., Chazdon, R., Ewers, R.M., Harvey, C.A., Peres, C.A., Sodhi, N.S., 2009.  
571 Prospects for tropical forest biodiversity in a human-modified world. *Ecology letters* 12, 561-582.

572 Geiger, R., 1954. Klassifikation der klimate nach W. Köppen. *Landolt-Börnstein-Zahlenwerte und*  
573 *Funktionen aus Physik, Chemie, Astronomie, Geophysik und Technik* 3, 603-607.

574 Goudriaan, J., 1977. *Crop micrometeorology: a simulation study*. Pudoc.

575 Greiser, C., Meineri, E., Luoto, M., Ehrlén, J., Hylander, K., 2018. Monthly microclimate models in a  
576 managed boreal forest landscape. *Agricultural and Forest Meteorology* 250, 147-158.

577 Hersbach, H., 2016. The ERA5 Atmospheric Reanalysis, AGU fall meeting abstracts.

578 Ingenhousz, J., 1779. Experiments upon vegetables: discovering their great power of purifying the  
579 common air in the sun-shine, and of injuring it in the shade and at night. To which is joined, a new  
580 method of examining the accurate degree of salubrity of the atmosphere. Printed by P. Elmsly and  
581 H. Payne.

582 Inoue, E., 1963. On the Turbulent Structure of Airflow within. *Journal of the Meteorological Society*  
583 *of Japan*. Ser. II 41, 317-326.

584 Jarvis, P.G., McNaughton, K.G., 1986. Stomatal control of transpiration: scaling up from leaf to region,  
585 *Advances in Ecological Research* 15, 1-49.

586 Kanamitsu, M., Ebisuzaki, W., Woollen, J., Yang, S.-K., Hnilo, J., Fiorino, M., Potter, G., 2002. Ncep-  
587 doe amip-ii reanalysis (r-2). *Bulletin of the American Meteorological Society* 83, 1631-1644.

588 Katul, G.G., Albertson, J.D., 1999. Modeling CO<sub>2</sub> sources, sinks, and fluxes within a forest canopy.  
589 *Journal of Geophysical Research: Atmospheres* 104, 6081-6091.

590 Kearney, M.R., Gillingham, P.K., Bramer, I., Duffy, J.P., Maclean, I.M., 2020. A method for computing  
591 hourly, historical, terrain-corrected microclimate anywhere on Earth. *Methods in Ecology and*  
592 *Evolution* 11, 38-43.

593 Kearney, M.R., Porter, W.P., 2017. NicheMapR—an R package for biophysical modelling: the  
594 microclimate model. *Ecography* 40, 664-674.

595 Kelliher, F.M., Leuning, R., Raupach, M., Schulze, E.-D., 1995. Maximum conductances for  
596 evaporation from global vegetation types. *Agricultural and Forest Meteorology* 73, 1-16.

597 Köppen, W., 1884. Die Wärmezonen der Erde, nach der Dauer der heissen, gemässigten und kalten Zeit  
598 und nach der Wirkung der Wärme auf die organische Welt betrachtet. *Meteorologische Zeitschrift*  
599 1, 5-226.

600 Körner, C., 1995. Leaf diffusive conductances in the major vegetation types of the globe,  
601 *Ecophysiology of photosynthesis*. Springer, pp. 463-490.

602 Kumarathunge, D.P., Medlyn, B.E., Drake, J.E., Tjoelker, M.G., Aspinwall, M.J., Battaglia, M., Cano,  
603 F.J., Carter, K.R., Cavaleri, M.A., Cernusak, L.A., 2019. Acclimation and adaptation components  
604 of the temperature dependence of plant photosynthesis at the global scale. *New Phytologist* 222,  
605 768-784.

606 Lee, X., Fuentes, J.D., Staebler, R.M., Neumann, H.H., 1999. Long-term observation of the atmospheric  
607 exchange of CO<sub>2</sub> with a temperate deciduous forest in southern Ontario, Canada. *Journal of*  
608 *Geophysical Research: Atmospheres* 104, 15975–15984.

609 Lembrechts, J.J., Lenoir, J., 2019. Microclimatic conditions anywhere at any time! *Global Change*  
610 *Biology*.

611 Lembrechts, J.J., Nijs, I., Lenoir, J., 2019. Incorporating microclimate into species distribution models.  
612 *Ecography* 42, 1267-1279.

613 Lenoir, J., Hattab, T., Pierre, G., 2017. Climatic microrefugia under anthropogenic climate change:  
614 implications for species redistribution. *Ecography* 40, 253-266.

615 Lompar, M., Lalić, B., Dekić, L., Petrić, M., 2019. Filling gaps in hourly air temperature data using  
616 debiased ERA5 data. *Atmosphere* 10, 13.

617 Lowman, M., Nadkarni, N., Mitchell, D., 1996. Forest canopies. *Biological Journal of the Linnean*  
618 *Society* 59, 217.

619 Maclean, I.M., 2020. Predicting future climate at high spatial and temporal resolution. *Global Change*  
620 *Biology* 26, 1003-1011.

621 Maclean, I.M., Mosedale, J.R., Bennie, J.J., 2019. Microclima: An R package for modelling meso-and  
622 microclimate. *Methods in Ecology and Evolution* 10, 280-290.

623 Maclean, I.M., Suggitt, A.J., Wilson, R.J., Duffy, J.P., Bennie, J.J., 2017. Fine-scale climate change:  
624 modelling spatial variation in biologically meaningful rates of warming. *Global Change Biology* 23,  
625 256-268.

626 McNaughton, K., Van den Hurk, B., 1995. A ‘Lagrangian’ revision of the resistors in the two-layer  
627 model for calculating the energy budget of a plant canopy. *Boundary-Layer Meteorology* 74, 261-  
628 288.

629 Meineri, E., Hylander, K., 2017. Fine- grain, large- domain climate models based on climate station  
630 and comprehensive topographic information improve microrefugia detection. *Ecography* 40, 1003-  
631 1013.

632 Michaletz, S.T., Weiser, M.D., McDowell, N.G., Zhou, J., Kaspari, M., Helliker, B.R., Enquist, B.J.,  
633 2016. The energetic and carbon economic origins of leaf thermoregulation. *Nature Plants* 2, 1–9.

634 Mitchell, J.W., 1976. Heat transfer from spheres and other animal forms. *Biophysical Journal* 16, 561-  
635 569.

636 Monin, A.S., Obukhov, A.M., 1954. Basic laws of turbulent mixing in the surface layer of the  
637 atmosphere. *Contrib. Geophys. Inst. Acad. Sci. USSR* 151, e187.

638 Monteith, J., Unsworth, M., 2013. *Principles of environmental physics: plants, animals, and the*  
639 *atmosphere*. Academic Press.

640 Monteith, J.L., 1965. Evaporation and environment. *Symposia of the Society for Experimental Biology*  
641 19, 205–224.

642 Munger, W., Hadley, J., 2020. Net Carbon Exchange of an Old-Growth Hemlock Forest at Harvard  
643 Forest HEM Tower since 2000. *Harvard Forest Data Archive* HF103.

644 Nabi, I., 1985. On the Tendencies of Motion, in: Levins, R., Lewontin, R. (eds.), *The Dialectical*  
645 *Biologist*. Harvard University Press, Cambridge, MA, pp. 124-126.

646 Nakamura, A., Kitching, R.L., Cao, M., Creedy, T.J., Fayle, T.M., Freiberg, M., Hewitt, C., Itioka, T.,  
647 Koh, L.P., Ma, K., 2017. Forests and their canopies: achievements and horizons in canopy science.  
648 *Trends in ecology & evolution* 32, 438-451.

649 Penman, H.L., 1948. Natural evaporation from open water, bare soil and grass. *Proceedings of the Royal*  
650 *Society of London. Series A. Mathematical and Physical Sciences* 193, 120-145.

651 Perez, T.M., Feeley, K.J., 2020. Photosynthetic heat tolerances and extreme leaf temperatures.  
652 *Functional Ecology* 00, 1–10.

653 Porter, W., Mitchell, J., Beckman, W., DeWitt, C., 1973. Behavioral implications of mechanistic  
654 ecology. *Oecologia* 13, 1-54.

655 Potter, K.A., Arthur Woods, H., Pincebourde, S., 2013. Microclimatic challenges in global change  
656 biology. *Global change biology* 19, 2932-2939.

657 Prandtl, L., 1925. Bericht über die Entstehung der Turbulenz. *Z. Angew. Math. Mech* 5, 136-139.

658 Raupach, M., 1989. Applying Lagrangian fluid mechanics to infer scalar source distributions from  
659 concentration profiles in plant canopies. *Agricultural and Forest Meteorology* 47, 85-108.

660 Raupach, M., Thom, A.S., 1981. Turbulence in and above plant canopies. *Annual Review of Fluid*  
661 *Mechanics* 13, 97-129.

662 Rebmann, C., Aubinet, M., Schmid, H., Arriga, N., Aurela, M., Burba, G., Clement, R., De Ligne, A.,  
663 Fratini, G., Gielen, B., 2018. ICOS eddy covariance flux-station site setup: a review.

664 Richardson, L., 1922. *Weather prediction by numerical process* (Cambridge U. Press). Dover  
665 Publications edition (1965) New York.

666 Shaw, R.H., Pereira, A., 1982. Aerodynamic roughness of a plant canopy: a numerical experiment.  
667 *Agricultural Meteorology* 26, 51-65.

668 Suggitt, A.J., Gillingham, P.K., Hill, J.K., Huntley, B., Kunin, W.E., Roy, D.B., Thomas, C.D., 2011.  
669 *Habitat microclimates drive fine-scale variation in extreme temperatures*. *Oikos* 120, 1-8.

670 Suggitt, A.J., Wilson, R.J., Isaac, N.J., Beale, C.M., Auffret, A.G., August, T., Bennie, J.J., Crick, H.Q.,  
671 Duffield, S., Fox, R., 2018. Extinction risk from climate change is reduced by microclimatic  
672 buffering. *Nature Climate Change* 8, 713.

673 Templer, P., Sanders-DeMott, R., Juice, S., Bowles, F., Sofen, L., Harrison, J., 2019. Climate Change  
674 Across Seasons Experiment (CCASE) at the Hubbard Brook Experimental Forest: Soil and  
675 Air Temperature. *Environmental Data Initiative*, v3. [https://doi.org/10.6073/PASTA/  
676 C6A9AC6C5CBC05888170902B8AF54869](https://doi.org/10.6073/PASTA/C6A9AC6C5CBC05888170902B8AF54869)

677 Teramoto, M., Liang, N., Takahashi, Y., Zeng, J., Saigusa, N., Ide, R., Zhao, X., 2019. Enhanced  
678 understory carbon flux components and robustness of net CO<sub>2</sub> exchange after thinning in a larch  
679 forest in central Japan. *Agricultural and Forest Meteorology* 274, 106–117.

680 Thimonier, A., Sedivy, I., Schleppi, P., 2010. Estimating leaf area index in different types of mature  
681 forest stands in Switzerland: a comparison of methods. *European Journal of Forest Research* 129,  
682 543-562.

683 Thomas, L., 1949. Elliptic problems in linear differential equations over a network: Watson scientific  
684 computing laboratory. Columbia Univ., NY.

685 Waggoner, P.E., Furnival, G., Reifsnnyder, W., 1969. Simulation of the microclimate in a forest. *Forest  
686 Science* 15, 37-45